RSC Advances

Shape-controlled synthesis of α-Fe2O3 nanocrystals for efficient adsorptive removal of Congo red

Journal:	*RSC Advances*
Manuscript ID:	RA-ART-04-2015-006324.R1
Article Type:	Paper
Date Submitted by the Author:	12-May-2015

Complete List of Authors:	Wang, Jintao; Nanjing Normal University, School of Chemistry and Materials Science Xu, Lei; Nanjing Normal University, School of Chemistry and Materials Science; Nanjing University, Chemistry Zhang, Zaiyong; Nanjing Normal University, School of Chemistry and Materials Science Sun, Peipei; Nanjing Normal University, School of Chemistry and Materials Science Fang, Min; Nanjing Normal University, School of Chemistry and Materials Science Liu, Hong-Ke; Nanjing Normal University, School of Chemistry and Materials Science

SCHOLARONE™
Manuscripts

RSC Advances

RSCPublishing

ARTICLE

Shape-controlled synthesis of α-Fe_2O_3 nanocrystals for efficient adsorptive removal of Congo red†

Cite this: DOI: 10.1039/xoxxoooooox

Jintao Wang,[#a] Lei Xu,[#a,b] Zaiyong Zhang,[a] Pei-Pei Sun,[a] Min Fang[a] and Hong-Ke Liu*[a]

Received ooth January 2012,
Accepted ooth January 2012

DOI: 10.1039/xoxxoooooox

www.rsc.org/

A facile solvothermal reaction was developed to synthetize α-Fe_2O_3 nanocrystals at relatively low temperature in the presence of small organic compound 2,4,6-Tris(pyrazol-1-yl)-1,3,5-triazine (Tptz) as template. α-Fe_2O_3 nanocrystals with three different morphologies were obtained by simply changing the volume ratio of the reaction solvents, *N,N*-dimethylformamide (DMF) and H_2O. The purities and morphologies of these samples were characterized by powder X-ray diffraction (PXRD), infrared spectrum (IR), high-resolution transmission electron microscopy (HRTEM) and field emission scanning electron microscopy (FESEM). It is remarkable that both the template Tptz ligand and the volume ratios of the mixture solvents are playing very significant roles for the formation and the morphological control of the products in this work. Furthermore, Congo red adsorption experiment showed that the adsorption capacities increased in an order of the samples with morphologies of nanopolyhedra, nanorods and rice-shaped. And the determined maximum adsorption capacity is up to 161 mg g^{-1} for the rice-shaped α-Fe_2O_3, which has the biggest BET surface area of 110.2 m^2g^{-1}. These α-Fe_2O_3 nanocrystals reported here may have the potential to use as low-cost and efficient adsorbent materials to remove organic pollutants from water.

Introduction

As the most thermodynamically stable form of iron oxides under ambient conditions and the most environmentally friendly n-type semiconductor with 1.9-2.2 eV band gap, hematite (α-Fe_2O_3) nanoparticles have broad potential applications in many fields, including photoelectrochemical water splitting, lithium ion batteries, and gas sensor.[1-8] Various methods have been developed for the controllable synthesis of hematite nanoparticles with certain morphologies, such as direct thermal decomposition,[9] sol-gel method,[10] hydrothermal,[11] and microwave-assisted method.[12] However, most of the methods usually involve multiple steps, special equipments, high temperature and also time-consuming. It is still a challenge to realize a facile method to prepare hematite nanoparticles with special morphologies.[13]

Physical and chemical interactions of organic functional groups with the surface of nanoparticles that often result in remarkable properties along with the stability and better dispensability, and some organic molecules are found to play key roles in the forming process of multimorphology hematite.[14] Even the template-assisted synthesis suffers from some disadvantages such as high cost, low yield and contamination from removal of the template,[15] it's still a useful method for obtaining α-Fe_2O_3 with unique structure. For example, Zhong et al.[16] utilized a solvothermal method to synthesize 3D flower-like hematite nanostructures by using an ethylene glycol-mediated self-assembly process. Xu et al.[17] successfully synthesized multishelled α-Fe_2O_3 hollow microspheres composed of hierarchical assemblies of 20–30 nm nanocrystals by using carbonaceous microsphere sacrificial templates. Hexadecyltrimethyl ammonium bromide (CTAB),[18,19] β-cyclodextrin[20] and urotropin[21] were also used to guide the generation of α-Fe_2O_3 with interesting structures. Moreover, Min et al[22] found that poly(vinyl pyrrolidone) plays a critical role for the formation of rhombohedra-like α-Fe_2O_3 nanoparticles, while *n*-decanoic acid and *n*-decylamine was used by Takami's group to control the shape of hematite nanoparticles.[23] Thus, synthesis of α-Fe_2O_3 nanostructures in the presence of organic compound as templates is a promising strategy for obtaining α-Fe_2O_3 nanoparticles with novel shape and function.

On the other hand, owing to the huge damage of water pollution, increasing attention has been paid to waste water treatment in the past few decades.[24-26] Among varies of conventional methods for water treatment, adsorption technique has been received favour due to the simplicity, high efficiency, and availability of a large number of adsorbents.[27-31] Currently, nanomaterials fabricated for adsorption applications in water treatment have gained considerable interest because that their large surface areas and rich valence states bring about enhanced adsorption performance. Among all kinds of nanomaterials, hematite (α-Fe_2O_3) nanoparticles has been becoming popular in the applications of removing toxic heavy metal ions and organic pollutants from waste water because that it is stable, eco-friendly, abundant, and inexpensive.[16,32-35] Herein we report a simple and mild method to synthesis multimorphology hematite

This journal is © The Royal Society of Chemistry 2014

nanoparticles at relatively low temperature. A small organic molecule Tptz which can be easily synthetized was used as template (Scheme 1). Moreover, through changing the ratios of the mixed solvents (DMF/H_2O), different morphology hematite nanoparticles are obtained, and results demonstrate that both Tptz and the mixed solvents play key roles in the formation of α-Fe_2O_3 nanoparticles with certain morphology.

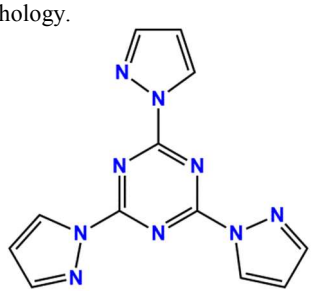

Scheme 1 Schematic drawing of the template compound Tptz.

Experimental section

General methods

Commercially available reagents were purchased from Sinopharm Chemical Reagent Co. Ltd. as analytical grade and used without further purification. Tptz was synthetized according to the reported method (ESI†).[36] IR spectra were recorded with an FT-IR spectrometer (Nicolet Nexus 670, USA) in the range of 400~4000 cm^{-1} on pressed disks using KBr as binding material. Crystal phase and structure of the samples were identified by the powder X-ray diffractometer (PXRD, D8-Advance, Bruker, Germany) with a scanning rate of 0.02 degree/s in the 2θ range of 10 ~ 90 degrees. Morphology and microstructure of the samples were examined by a transmission electron microscopy (TEM, H-7650, Hitachi, Japan); high resolution transmission electron microscopy (HRTEM, JEM-2010, JEOL, Japan) and field emission scanning electron microscopy (SEM, JSM 7401F, JEOL, Japan). A Varian Cary 50 Probe UV-vis spectrophotometer was used for UV scanning.

Synthesis of α-Fe_2O_3 nanoparticles

A total volume of 8 mL solvent with mixed DMF and distilled water of different volume ratios (DMF:H_2O = 1:3, 1:1 and 3:1) were added into the glass vessel containing $FeCl_3 \cdot 6H_2O$ (54 mg 0.2 mmol) and Tptz (55.8 mg 0.2 mmol). After stirring till the solution turns clear, the glass vessel was transferred into a Teflon-lined stainless-steel autoclave for hydrothermal treatment at 100 °C for 24 h. Then, the autoclave was cooled down to room temperature naturally. The resulted precipitate was collected and washed by DMF, H_2O, ethanol and diethyl ether, and finally dried.

Porosity Analysis

Gas adsorption isotherms were collected by a volumetric method using Micromeritics ASAP 2020 sorption analyzer. N_2 Gas adsorption isotherms were measured at 77 K using a liquid N_2 bath. Before measurement, the samples were activated in the analysis tube under vacuum using the "degas" function of the adsorption analyzer at 150 °C for 12 h.

Removal of Congo red

Congo red ($C_{32}H_{22}N_6O_6S_2Na_2$), which is an azo dye that widely used in the textile industry, was commonly selected as a model organic water pollutant. In a typical process, a 50 mL mixture containing the final concentration of 100 mg/L Congo red and 600 mg/L α-Fe_2O_3 was mixed thoroughly in a tube at 25 °C during the daytime. At several time intervals, 3 mL of dye solution was taken out and immediately separated by centrifugation. Then, the removal of CR dye was monitored by measuring the maximum adsorption peak at 497 nm using UV-vis spectrometer. With the same concentrations of CR and α-Fe_2O_3, the effect of pH on adsorption was studied in a pH range of 4.0–10.0. And the initial pH was adjusted by adding aqueous solutions of 0.01 M HCl or 0.01 M NaOH. For the CR regeneration experiment, α-Fe_2O_3 samples were separated from the mixture by centrifuging after every three hours adsorption of CR, and washed with ethanol at least three times under ultrasonic to remove the adsorptive CR as much as possible, and finally washed with water and reused for the next run.

Results and discussion

Structure Characterization.

The purity and crystallinity of α-Fe_2O_3 samples were determined using powder XRD measurements (Fig. 1). Fig. 1a-c show the XRD patterns of the as-prepared α-Fe_2O_3 nanopolyhedra (A1), α-Fe_2O_3 nanorods (A2) and rice-shaped α-Fe_2O_3 (A3), obtained by hydrothermal method at 100 °C with the solvent DMF/H_2O volume of 2 mL/6 mL, 4 mL/4 mL and 6 mL/2 mL, respectively. It is evident that all of the expected peaks can be indexed to the stick pattern (JCPDS No. 033-0664) of pure hematite and no impurity peaks for FeOOH, Fe_3O_4 or γ-Fe_2O_3 observed. Further evidence for the formation of α-Fe_2O_3 can be obtained from the FT-IR spectra of the samples. As shown in Fig. S1 (see the Supporting Information), the distinct peaks at 3450 and 1615 cm^{-1} are the vibrations of H_2O. Another small peak at 1390 cm^{-1} is ascribed to bending frequency of surface hydroxyl group.[37] While the other two important peaks at 472 and 553 cm^{-1} are the characteristic vibrations in the α-Fe_2O_3 product,[38] indicating the formation of the α-Fe_2O_3 phase. Besides, FT-IR spectra of all A1, A2 and A3 are very similar, indicating they should contain the same component. Thus, both XRD and FT-IR results clearly show that pure α-Fe_2O_3 species are obtained under present experimental condition.

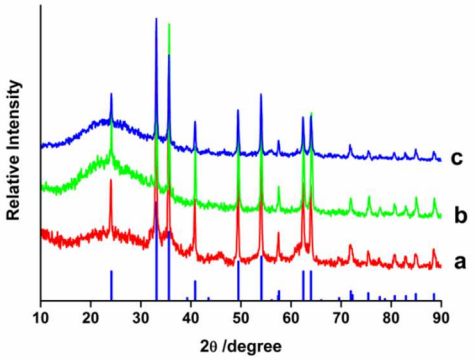

This journal is © The Royal Society of Chemistry 2012

Fig. 1 Powder X-ray diffraction (PXRD) pattern of the synthesized samples: (a) A1, α-Fe_2O_3 nanopolyhedra; (b) A2, α-Fe_2O_3 nanorods; (c) A3, rice-shaped α-Fe_2O_3. The standard powder pattern of hematite (Powder Diffraction File number (PDF#) 033-0664) was at the bottom.

Shape-controlled by the solvent

Solvent are the essential factor in the formation of α-Fe_2O_3 nanostructure. In this study we synthesized the α-Fe_2O_3 with mixed solvents DMF/H_2O of different ratios in the present of template Tptz. Actually, absolutely DMF or H_2O was used to perform the solvothermal reaction initially. There were no crystals or precipitates when the reaction was performed in DMF, but rice-shaped nanomaterials were obtained (Fig. S2) while pure H_2O was used as the solvent. The size of above homogeneous nanorods obtained in water is 250 nm in length and 50 nm in width. Interestingly, TEM figures show that these nanorods are core–shell like structure. However, the result from PXRD analysis (Fig. S3) indicates that these obtained nanorods are not pure α-Fe_2O_3, γ-Fe_2O_3 or FeOOH. Probably this unknown nanorods material is a mixture of α-Fe_2O_3 and FeOOH because it needs a much longer time to accomplish the transformation from $FeCl_3$ to α-Fe_2O_3 at relative low hydrolytic temperature,[39] otherwise FeOOH will come out as the main product.[40]

Then we synthesized α-Fe_2O_3 nanoparticles by using mixed solvents DMF/H_2O of different volume ratios (typically, DMF:H_2O = 1:3, 1:1 and 3:1). Fortunately, pure α-Fe_2O_3 with three different morphologies were obtained in these mixed solvents by using Tptz as template, and field emission scanning electron microscope (FESEM), transmission electron microscopy (TEM) and high-resolution transmission electron microscopy (HRTEM) experiments were proceed to extensively investigate the morphology of the nanostructures.

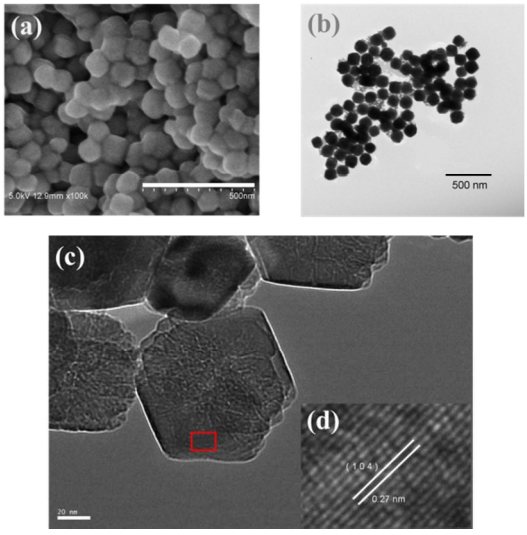

Fig. 2 (a) TEM image, (b) FESEM image, (c) HRTEM image and (d) HRTEM image of the denoted region in Fig. 2c of the as-prepared α-Fe_2O_3(A1) in DMF/H_2O (2 mL/6 mL) with 0.2 mmol Tptz at 100 ^oC.

Fig. 2 included the SEM and TEM (HRTEM) images of α-Fe_2O_3 (A1) that was obtained from mixed solvents of DMF/H_2O (2 mL/6 mL). As shown in Fig 2a and 2b, the homogeneous and solid nanoparticles displayed a morphology of nanopolyhedra with the size of 110 nm that calculated by Nano Measurer 1.2.5 software (add a reference here). Furthermore, hexagonal shaped α-Fe_2O_3 nanoparticles were visibly found from HRTEM image in Fig. 2c. The typical lattice fringe spacing was 0.27 nm (Fig. 2d), corresponding to the (104) hexagonal plane of α-Fe_2O_3.

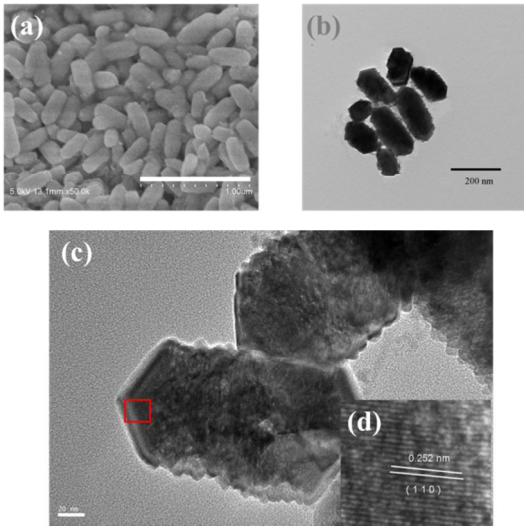

Fig. 3 (a) TEM image, (b) FESEM image, (c) HRTEM image and (d) HRTEM image of the denoted region in Fig. 3c of the as-prepared α-Fe_2O_3 (A2) in DMF/H_2O (4 mL/ 4mL) with 0.2 mmol Tptz at 100 ^oC.

When the DMF/H_2O volume ratio was changed to 4 mL/4 mL, a quite different morphology of α-Fe_2O_3 (A2) was obtained. As shown in Fig 3a and 3b, α-Fe_2O_3 with shape of nanorods was the main product. The calculated averaged length and width of the nanorods were 300 and 135-150 nm, respectively. Interestingly, all the nanorods contained two obtuse angles of 115° in both ends. The typical lattice fringe spacing shown in HRTEM image (Fig. 3d) was determined to be 0.252 nm, corresponding to the (110) lattice plane of α-Fe_2O_3.

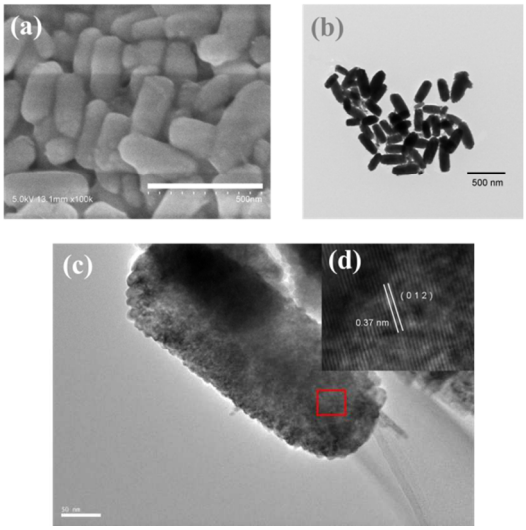

Fig. 4 (a) TEM image, (b) FESEM image, (c) HRTEM image and (d) HRTEM image of the denoted region in Fig. 4c of the as-prepared α-Fe_2O_3 (A3) in DMF/H_2O (6 mL/2 mL) with 0.2 mmol Tptz at 100 ^oC.

More interestingly, rice-shaped α-Fe_2O_3 nanoparticles were obtained (A3) when DMF/H_2O ratio of the mix solvents was changed to 6: 2. As shown in Fig. 4a and 4b, the shape of A3 was similar to that of A2 except there was no angle in the terminal. Besides, the width of A3 was 135 nm, which was very close to A2. While the length of A3 was 350 nm, it was a little bit longer than that of A2. It was also indicated obviously that the lattice fringe with interplanar spacing was 0.37 nm (Fig. 4d), corresponding to the (012) plane of the crystalline hematite.

Considering that there was no pure and well-crystallized α-Fe_2O_3 obtained when the reaction was performed in solely DMF or H_2O, we found that both DMF and H_2O play important roles during the formation of crystalline hematite. On the other hand, by changing the ratios of DMF/H_2O in the mix solvents, α-Fe_2O_3 nanoparticles with three different morphologies have been obtained in the presence of Tptz. Characterization of the nanoparticles by TEM, HRTEM and FESEM indicate that these nanoparticles are well crystallized and belong to single crystalline. Hence, shape-controlled synthesis of α-Fe_2O_3 nanoparticles is achieved by simply varying the ratios of DMF and H_2O.

Shape-controlled by the template Tptz

Apart from solvent, there are several other factors that are important for the formation of α-Fe_2O_3 nanocrystals. In the present research, 2,4,6-Tris(pyrazol-1-yl)-1,3,5-triazine (Tptz) was used as the template compound. Initially, we tried to synthesize the α-Fe_2O_3 in the absence of any template compounds with mix solvent DMF/H_2O of different ratios (DMF:H_2O = 1:3, 1:1 and 3:1) at 100 ^oC for 24 hours. The resulted products were shown in Fig. 5, and XRD measurements were performed to characterize these nanomaterials (Fig. S4). Results showed that all three samples were pure α-Fe_2O_3, indicating that the transition from $FeCl_3$ to α-Fe_2O_3 is active in our experimental conditions even without any external template. However, the product were not well shaped. For instance, the particles in Fig. 5a are relative small and messy. Meanwhile, all the samples were not homogeneous and quite different from that of nanocrystals A1, A2 and A3, indicating that the Tptz did plays a significant role in the formation of homogeneous α-Fe_2O_3.

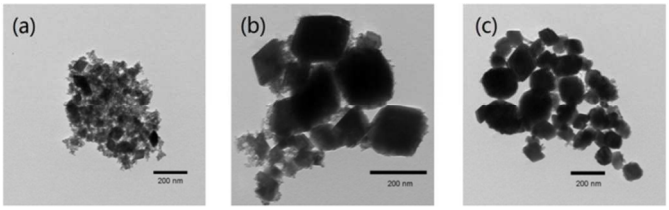

Fig. 5 TEM images of the products from the reactions without Tptz in the mix solvent DMF/H_2O of different volume ratios: (a) 2 mL/6 mL, (b) 4 mL/4 mL and (c) 6 mL/2 mL.

As described before, the nanocrystals of A1, A2 and A3 were synthesized with template Tptz of 0.2 mmol. In order to study how the amounts of template affect the formation of products, we have performed reactions by only changing the amount of Tptz, but keeping the reaction temperature (100 ^oC) and time (24 h) unchanged. As shown in Fig. S5, the shapes of the samples obtained from solvents with DMF/H_2O ratios of 2 mL/6 mL, 4 mL/4 mL and 6 mL/2 mL changed dramatically, when the amounts of Tptz were varied from 0.1 to 0.5 mmol, respectively. For example, when 0.1 mmol Tptz was used, the shapes of three resulted α-Fe_2O_3 were similar to that of A1, A2 and A3, respectively, which were obtained from the reactions with 0.2 mmol Tptz. However, the nanostructures of these α-Fe_2O_3 were not crystallized well. There were some interesting observations for the shapes and sizes of the resulted α-Fe_2O_3 when the amount of Tptz were increased. That was, the sizes of those α-Fe_2O_3 nanoparticles were became bigger, together with the shapes were turned to oval-shaped nanocrystals (Fig. 5). For example, the SEM images clearly showed that the sizes of nanocrystal formed in the presence of 0.5 mmol Tptz and DMF/H_2O (6 mL/2 mL), were 400 nm in length and 200 nm in width, which was quite different from that of A3, in which the length and width were 350 nm and 135 nm, respectively. Furthermore, when 0.5 mmol Tptz was used in the three parallel reactions, all the resulted products displayed similar oval-shaped nanostructure. These results may suggest that the excess amount of Tptz could neutralize the effects of the mixed solvent, and further induce the formation of α-Fe_2O_3 nanocrystals with analogous shapes. Thus, it is obvious that the nanostructures of α-Fe_2O_3 are highly dependent on concentrations of Tptz.

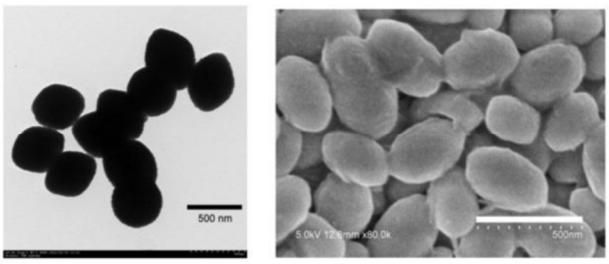

This journal is © The Royal Society of Chemistry 2012

Fig. 6 (a) TEM image, (b) FESEM image of the as-prepared α-Fe_2O_3 in DMF/H_2O (6 mL/2 mL) with 0.5 mmol Tptz at 100 °C for 24 h.

Formation Mechanism

Hydrothermal method is considered to be the best technique to control nanostructures of different shapes and sizes. Various morphological nanoparticles have been fabricated with this method.[41-42] However, the formation mechanism of nanoparticles with different shapes have not been well established to date, herein we have tried to make some attempts to propose the mechanism for α-Fe_2O_3. First of all, the pyrazolyl-derivative Tptz is considered as the alkaline reagent. The OH^- ions formed as a result of the hydrolysis of Tptz under hydrothermal condition (equation 1) and further resulted in homogeneous precipitation of $Fe(OH)_3$/FeOOH. Then, α-Fe_2O_3 particles were formed from the $Fe(OH)_3$/FeOOH by topochemical phase transformation. That the very low solubility of $Fe(OH)_3$ might be the cause to make the transformation of Fe_2O_3 from $Fe(OH)_3$ (equation 2).[43] Eventually, the template Tptz might play a key role in facilitating the formation of uniform iron oxide nanostructures as a stabilizer and modifier as well as a hydrolyzing agent and other additive agents.[44-46] Thus, the progressive hydrolysis of Tptz made the solution alkaline and induced homogeneous nucleation, hydroxide precipitation, and crystallization of metal species. In regard to the influences of template amounts on the morphologies of the products, we might suggest that the release speed and the amount of OH^- were significantly affected by concentrations of Tptz, which would further influence the nucleation and transformation steps.

$$Tptz + H_2O \rightarrow H_3Tptz^{3+} + 3OH^- \quad (1)$$

$$FeCl_3 + 3OH^- \rightarrow Fe(OH)_3/FeOOH \rightarrow \alpha\text{-}Fe_2O_3 \quad (2)$$

Wastewater treatment

Generally, metal oxide nanostructure materials with high specific surface areas can be used as adsorbents to remove pollutants from waste water. Compared with other adsorbents such as activated carbon, metal oxide nanostructure systems will be more promising due to the feasible regeneration by catalytic combustion at relatively low temperatures.[47] Congo red (CR), a common dye in textile industry, is selected as the organic contaminant in the waste water. In the solution, Congo red is adsorbed onto α-Fe_2O_3 surface by coordination effect between metal ions and amine groups at the ends of CR molecules.

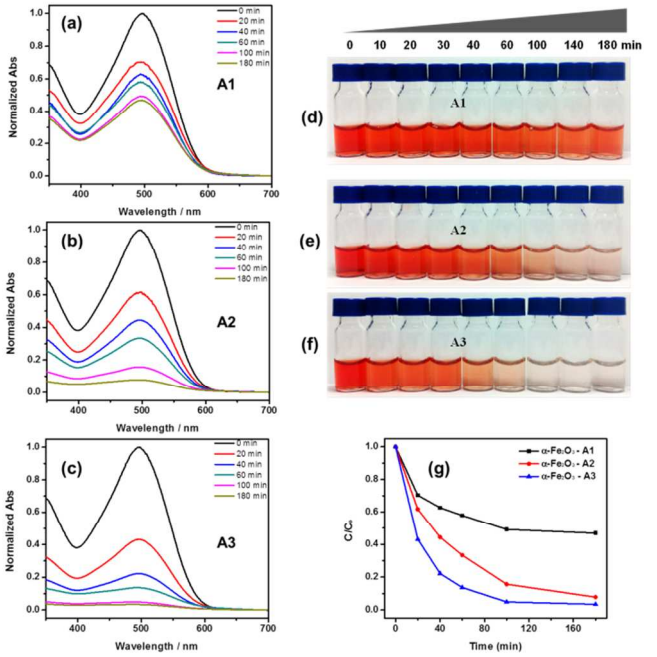

Fig. 7 (a), (b) and (c) are time-dependent UV-vis adsorption spectra of CR solutions treated by α-Fe_2O_3 nanostructures A1, A2 and A3, respectively; (d), (e) and (f) are pictures of CR after treated by A1, A2 and A3 at different periods of time; (g), adsorption rate of CR on the as-prepared α-Fe_2O_3 A1, A2 and A3.

UV-vis adsorption spectroscopy was used to record the adsorption behaviour of the CR solution after treated with α-Fe_2O_3 (Fig. 7). The characteristic adsorption band of CR at 497 nm was chosen to monitor the process of adsorption and results were shown in Fig. 7. The adsorption spectra of the CR solutions (with an initial concentration of 100 mg L^{-1}) after treatment with 600 mg/L α-Fe_2O_3 A1, A2 and A3 with different time intervals were shown in Fig.7a-c, and pictures in Fig. 7d-f indicated that the fading of CR along with the increasing incubation time were observed obviously for samples A1-A3. However, the adsorption efficiency of A2 and A3 are much higher than that of A1. Furthermore, results also indicated that about 53%, 92% and 97% of the CR were removed by A1, A2 and A3 within 180 min, respectively (Fig. 7g). The maximum adsorption capacity of CR for A1-A3 were calculated to be 89, 154 and 161 mg g^{-1}, respectively. Literature survey indicates that the maximum adsorption capacity of the present samples may be comparable to or even higher than the majority of reported α-Fe_2O_3 materials[32,48-50] and some other reported nanomaterials, such as hierarchical hollow MnO_2 (80 mg g^{-1}),[23] hierarchical spindle-like γ-Al_2O_3 (90 mg g^{-1}),[49-51] and activated carbon (laboratory grade, 1.88 mg/g).[38] It is interesting to note that the order of crystallite size of A1-A3 (A1 < A2 < A3) is positively correlated to their adsorption activities, indicating that the crystallite size may be important for the CR adsorption.[45,46] Moreover, in order to clearly understand the relationship between the structure-activity relationships, nitrogen adsorption experiment was proceeded and the calculated Brunauer Emmett Teller (BET) surface areas for A1, A2 and A3 were 22.2,

46.5 and 110.2 m^2g^{-1} respectively (Fig. S6), which correspond well to theirs CR adsorption capacities.

Considering the regeneration of adsorbent is a very important characteristic, herein the best adsorbent, A3, was chosen for the regenerative investigation. As shown in Fig. S7, the CR removal efficiency decreased along with the reused times. After five times reuse of A3, the removal efficiency reduced from 98% to 32%, that indicated absolute regeneration of the CR removal efficiency of the as-prepared A3 cannot be achieved. From the experimental observation, we suggested the major problem was fully wash away the adsorbed CR in A3 nanocrystals was very hard in our present experimental conditions.

The pH value affect the chemistry of both CR and the adsorbent materials. Simultaneously, it also plays an important role in the adsorption capacity of adsorbent, that because it affects the surface charge of adsorbent, the degree of ionization of different pollutants, the dissociation of functional groups on adsorbent as well as the structure of the dye molecule.[52] The result of pH dependence of CR adsorbed by A3 is shown in Fig. 8. It's obvious that the adsorption efficiency was well kept ≥95% in a pH range of 4.0-8.0. Meanwhile, as the pH increased to 9.0 and 10.0, the removal efficiency decreased partially. That's mainly because at higher pH values, existence of a lot of negative charges on the surfaces of nanoparticles could lead to the electrostatic repulsion between A3 and CR, which as a dipolar molecular, exists as anionic form at basic pH and as cationic form at acidic pH conditions.[53] Then, the as-prepared α-Fe_2O_3 exhibit higher removal efficiency under acidic and neutral conditions rather than in alkaline condition. Thus, due to the excellent removal activity, the α-Fe_2O_3 nanoparticles reported here might be useful in the wastewater treatment and purification fields.

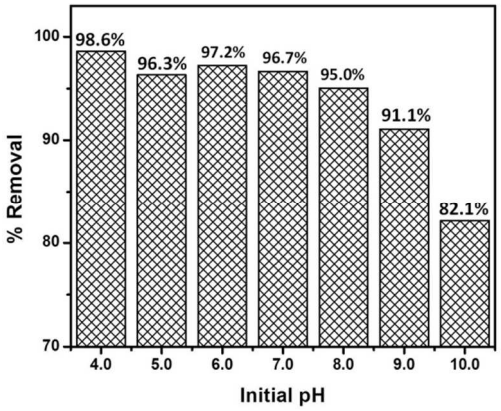

Fig. 8 Effect of initial solution pH of CR on the adsorption efficiency of α-Fe_2O_3 A3.

Conclusions

In summary, α-Fe_2O_3 structures of different morphologies have been synthesized by using a convenient, simple hydrothermal approach at relatively low temperature. It is remarkable that not only the ratios of DMF/water in mix solvents, but also the template compound Tptz together with the amount of Tptz play key roles for the formation of hematite nanoparticles with different shapes and sizes. An initial formation mechanism is proposed in this work and the presence of alkaline compound Tptz may be favorable for the generation of OH^- in the synthetic process, which is important for the formation of α-Fe_2O_3 nanoparticles by topochemical phase transformation. The high removal capacities of A1-A3 for Congo red, demonstrates that they should be promising candidates as adsorbent for wastewater treatment. These findings may benefit not only for further investigate of α-Fe_2O_3 nanoparticles with different morphologies, but the application on waste water treatment as well.

Acknowledgements

We thank the Key International (Regional) Joint Research Program of NSFC (Grant No. 21420102002), NSFC (Project 21171095, 21401105), the Specialized Research Fund for the Doctoral Program of Higher Education (SRFDP) of China (20123207110007), the Priority Academic Program Development of Jiangsu Higher Education Institutions (PAPD), the "Summit of the Six Top Talents" Program of Jiangsu Province for their support.

Notes and references

[a]Bio-Functional Material Key Lab of Jiangsu Province, Jiangsu Collaborative Innovation Center of Biomedical Functional Materials, School of Chemistry and Materials Science, Nanjing Normal University, Wenyuan Road 1, Nanjing 210023, PR China. E-mail: liuhongke@njnu.edu.cn

[b]School of Chemistry and Chemical Engeering, Nanjing University, Hankou Road 22, Nanjing 210068, PR China.

[#]These authors contributed equally to this work.

† Electronic Supplementary Information (ESI) available: Synthesis of Tptz, the FT-IR spectrum of the obtained products A1, A2 and A3, TEM images of the products obtained from pure H_2O, and from different solvent DMF/H_2O in the presence of 0.1-0.5 mmol Tptz, PXRD patterns of the synthesized samples in the absence of Tptz in three kinds of mixed solvent DMF/H_2O, recycle test of CR removal efficiency of A3. See DOI: 10.1039/b000000x/

1 J. Chen, L. Xu, W. Li and X. Gou, *Adv. Mater.*, 2005, **17**, 582-586.
2 A. Kay, I. Cesar and M. Grätzel, *J. Am. Chem. Soc.*, 2006, **128**, 15714-15721.
3 G. Wang, X. Gou, J. Horvat and J. Park, *J. Phys. Chem. C*, 2008, **112**, 15220-15225.
4 J. S. Chen, T. Zhu, X. H. Yang, H. G. Yang and X. W. Lou, *J. Am. Chem. Soc.*, 2010, **132**, 13162-13164.
5 K. Sivula, R. Zboril, F. Le Formal, R. Robert, A. Weidenkaff, J. Tucek, J. Frydrych and M. Grätzel, *J. Am. Chem. Soc.*, 2010, **132**, 7436-7444.
6 Y. J. Lin, G. B. Yuan, S. Sheehan, S. Zhou and D. W. Wang, *Energy Environ. Sci.*, 2011, **4**, 4862-4869.
7 B. Wang, J. S. Chen, H. B. Wu, Z. Wang and X. W. Lou, *J. Am. Chem. Soc.*, 2011, **133**, 17146-17148.
8 Z. Padashbarmchi, A. H. Hamidian, H. Zhang, L. Zhou, N. Khorasani, M. Kazemzad and C. Yu, *RSC Advances*, 2015, **5**, 10304-10309.

 This journal is © The Royal Society of Chemistry 2012

9 E. Darezereshki, *Mater. Lett.*, 2011, **65**, 642-645.
10 I. Opacak, M. Ristic and S. Music, *Mater. Lett.*, 2010, **64**, 2555-2558.
11 X. Wang, J. Zhuang, Q. Peng and Y. Li, *Nature*, 2005, **437**, 121-12.
12 X. Hu and J. C. Yu, *Adv. Funct. Mater.*, 2008, **18**, 880-887.
13 H. Ni, Y. H. Ni, Y. Y. Zhou and J. M. Hong, *Mater. Lett.*, 2012, **73**, 206-208.
14 Y. Khan, S. K. Durrani, M. Siddique and M. Mehmood, *Mater. Lett.*, 2011, **65**, 2224-2227.
15 X. D. Zheng and J. L. Li, *Ionics*, 2014, **20**, 1651-1663.
16 L. S. Zhong, J. S. Hu, H. P. Liang, A. M. Cao, W. G. Song and L. J. Wan, *Adv. Mater.*, 2006, **18**, 2426-2431.
17 S. M. Xu, C. M. Hessel, H. Ren, R. B. Yu, Q. Jin, M. Yang, H. J. Zhao and D. Wang, *Energ. Environ. Sci.*, 2014, **7**, 632-637.
18 S. Bharathi, D. Nataraj, M. Seetha, D. Mangalaraj, N. Ponpandian, Y. Masuda, K. Senthil and K. Yong, *CrystEngComm*, 2010, **12**, 373-382.
19 B. Jia and L. Gao, *Cryst. Growth Des.*, 2008, **8**, 1372-1376.
20 L. B. Wang, L. X. Song, Z. Dang, J. Chen, J. Yang and J. Zeng, *CrystEngComm*, 2012, **14**, 3355-3358.
21 A. Šarić, S. Musić, K. Nomura and S. Popović, *Mater. Sci. Eng., B*, 1998, **56**, 43-52.
22 C.-Y. Min, Y.-d. Huang and L. Liu, *Mater. Lett.*, 2007, **61**, 4756-4758.
23 S. Takami, T. Sato, T. Mousavand, S. Ohara, M. Umetsu and T. Adschiri, *Mater. Lett.*, 2007, **61**, 4769-4772.
24 J. B. Fei, Y. Cui, X. H. Yan, W. Qi, Y. Yang, K. W. Wang, Q. He and J. B. Li, *Adv. Mater.*, 2008, **20**, 452-456.
25 X. Qin, L. Jing, G. Tian, Y. Qu and Y. Feng, *J. Hazard. Mater.*, 2009, **172**, 1168-1174.
26 M. Rahsepar, M. Pakshir, Y. Piao and H. Kim, *Electrochim. Acta*, 2012, **71**, 246-251.
27 L. Wang and A. Wang, *J. Hazard. Mater.*, 2007, **147**, 979-985.
28 L. Wang, J.-T. Yang and P.-C. Lyu, *Chem. Eng. Sci.*, 2007, **62**, 711-720.
29 F. A. Pavan, S. L. P. Dias, E. C. Lima and E. V. Benvenutti, *Dyes. Pigm.*, 2008, **76**, 64-69.
30 A. Afkhami, T. Madrakian and A. Amini, *Desalination*, 2009, **243**, 258-264.
31 S. Lan, N. Guo, L. Liu, X. Wu, L. Li and S. Gan, *Appl. Surf. Sci.*, 2013, **283**, 1032-1040.
32 X. L. Fang, C. Chen, M. S. Jin, Q. Kuang, Z. X. Xie, S. Y. Xie, R. B. Huang and L. S. Zheng, *J. Mater. Chem.*, 2009, **19**, 6154-6160.
33 C. Yu, X. Dong, L. Guo, J. Li, F. Qin, L. Zhang, J. Shi and D. Yan, *J. Phys. Chem. C*, 2008, **112**, 13378-13382.
34 D. Zhu, J. Zhang, J. Song, H. Wang, Z. Yu, Y. Shen and A. Xie, *Appl. Surf. Sci.*, 2013, **284**, 855-861.
35 T. Hao, C. Yang, X. Rao, J. Wang, C. Niu and X. Su, *Appl. Surf. Sci.*, 2014, **292**, 174-180.
36 D. Azarifar, M. A. Zolfigol and A. Forghaniha, *Heterocycles*, 2004, **63**, 1897-1901.
37 J. R. Quinan and S. E. Wiberley, *Anal. Chem.*, 1954, **26**, 1762-1764.
38 F. Jones, J. B. Farrow and W. van Bronswijk, *Langmuir*, 1998, **14**, 6512-6517.
39 E. Lorenc-Grabowska and G. Gryglewicz, *Dyes. Pigm.*, 2007, **74**, 34-40.
40 T. P. Almeida, M. Fay, Y. Zhu and P. D. Brown, *J. Phys. Chem. C*, 2009, **113**, 18689-18698.
41 T. P. Almeida, M. Fay, Y. Zhu and P. D. Brown, *J. Phys. Chem. C*, 2009, **113**, 18689-18698.
42 N. G. Ndifor-Angwafor and D. J. Riley, *Phys. Status Solidi A*, 2008, **205**, 2351-2354.
43 T. Sugimoto, *Adv. Colloid Interface Sci.*, 1987, **28**, 65-108.
44 N. K. Chaudhari, H. Chan Kim, D. Son and J.-S. Yu, *CrystEngComm*, 2009, **11**, 2264-2267.
45 G. K. Pradhan and K. M. Parida, *ACS Appl. Mater. Interfaces*, 2011, **3**, 317-323.
46 W.-F. Tan, Y.-T. Yu, M.-X. Wang, F. Liu and L. K. Koopal, *Cryst. Growth Des.*, 2013, **14**, 157-164.
47 F. Herrera, A. Lopez, G. Mascolo, P. Albers and J. Kiwi, *J. Appl. Catal., B*, 2001, **29**, 147-162.
48 A. Afkhami and R. Moosavi, *J. Hazard. Mater.*, 2010, **174**, 398-403.
49 J. Fei, Y. Cui, J. Zhao, L. Gao, Y. Yang and J. Li, *J. Mater. Chem.*, 2011, **21**, 11742-11746.
50 Z. Wei, R. Xing, X. Zhang, S. Liu, H. Yu and P. Li, *ACS Appl. Mater. Interfaces*, 2012, **5**, 598-604.
51 W. Cai, J. Yu and M. Jaroniec, *J. Hazard. Mater.*, 2010, **20**, 4587-4594.
52 Y. Hu, H. Luo and H. Luo, *Sep. Sci. and Technol.*, 2014, **49**, 2700-2710.
53 H. Y. Zhua, Y. Q. Fu, R. Jiang, J. H. Jiang, L. Xiao, G. M. Zeng, S. L. Zhao and Y. Wang, *Chem. Eng. J.*, 2011, **173**, 494–502.

Contents Entry

Shape-controlled synthesis of α-Fe_2O_3 nanocrystals for efficient adsorptive removal of Congo red

Jintao Wang, Lei Xu, Zaiyong Zhang, Pei-Pei Sun, Min Fang and Hong-Ke Liu

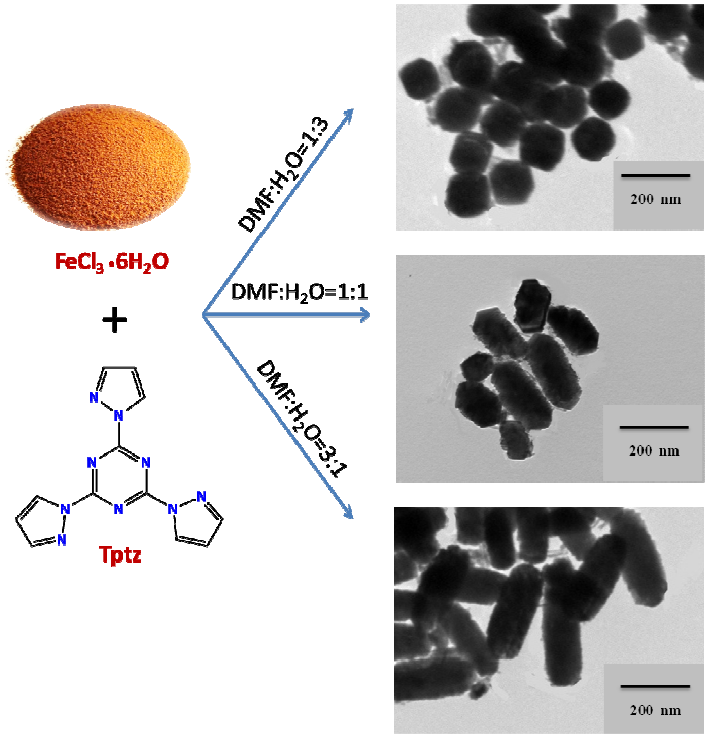

α-Fe_2O_3 nanocrystals of different sizes and morphologies have been obtained at relatively low temperature with Tptz as template, and the Congo red can be efficient removed by these nanocrystals.